Automatic Generation Control with Virtual Synchronous Renewables

Weichao Zhang, *Member*, *IEEE*, Wanxing Sheng, *Senior Member*, *IEEE*, Qing Duan, *Member*, *IEEE*, Hanyan Huang, *Student Member*, *IEEE*, and Xiangwu Yan, *Member*, *IEEE*

***Abstract*—As synchronous generators (SGs) are gradually displaced by renewable energy sources (RESs), the frequency stability of power systems deteriorates because RESs, represented by utility-scale solar and wind power sources, do not provide the inertial response, primary frequency response, secondary frequency response, and tertiary frequency regulation. As a result, the remaining SGs may not be sufficient to maintain the power balance and frequency stability. The concept and control strategies of virtual synchronous generators (VSGs) enable the inverter-based wind and solar power sources to emulate the outer characteristics of traditional SGs and participate in the active power and frequency control of power systems. This paper focuses on the automatic generation control (AGC) with virtual synchronous renewables (VSRs). First, the VSR strategy that enables the RESs to participate in AGC is introduced. Second, based on the interval representation of uncertainty, the output of RES is transformed into two portions, i.e., the dispatchable portion and the stochastic portion. In the dispatchable portion, the RESs can participate in AGC jointly with SGs. Accordingly, a security-constrained economic dispatch (SCED) model is built considering the RESs operating in VSR mode. Third, the solution strategy that employs the slack variables to acquire deterministic constraints is introduced. Finally, the proposed SCED model is solved based on the 6-bus and 39-bus systems. The results show that, compared with the maximum power point tracking (MPPT) mode, VSRs can participate in the active power and frequency control jointly with SGs, increase the maximum penetration level of RESs, and decrease the operating cost.**

***Index Terms*—Automatic generation control (AGC), economic dispatch, renewable energy source (RES), virtual synchronous generator (VSG).**

NOMENCLATURE

A. Indices and Notations

base	Superscript for base generation
D	Subscript for demand
DS	Subscript for dispatable source
fore	Superscript for forecasting value
G	Subscript for synchronous generators (SGs)
head	Superscript for regulation headroom
i, *j*, *k*, *l*, *n*	Indices for dispatchable sources, renewable energy sources (RESs), demands, lines, and buses
MPPT	Superscript for the maximum power point tracking (MPPT)
pene	Subscript for penetration
percent	Subscript for utilization percentage
R	Subscript for RESs
ref	Superscript for reference values
t	Index for time slots
upward	Superscript for upward reserves
VSR	Subscript for dispatchable portion of RESs in VSR mode

B. Parameters

$(\cdot)_m$	The m^{th} row of matrix $(\cdot)$
$\mathbf{1}^1$, $\mathbf{1}^2$	$N_{DS} \times N_R$ and $N_{DS} \times N_D$ matrices with all elements equal to 1
ε'_{Rj}	Power deviation of stochastic portion of RES j from forecasting power
ε_{Rj}, ε_{Dk}	Power deviation of RES j and demand k from forecasting power
ζ_{Rj}, ζ_{Dk}	Power deviation bounds of RES j and demand k
η_{Rj}, η_{Rj}^{fore}	Actual and forecasting power of stochastic portion of RES j
σ_{Rj}	Standard deviation of forecasting error of RES j
a_i, b_i, c_i	Fuel cost coefficients of generator i
$\boldsymbol{I}$	$N_{DS} \times N_{DS}$ identity matrix
I_{ni}^1, I_{nj}^2, I_{nk}^3	Relevance parameters of generator i, RES j, and demand k to bus n
L_{ln}	Power transfer distribution factor of bus n to

Manuscript received: December 29, 2020; revised: May 26, 2021; accepted: December 28, 2021. Date of CrossChecked: December 28, 2021. Date of online publication: February 11, 2022.

This work was supported by the Research and Application of Key Technologies of Flexible Power Supply System Under Various Emergency Scenarios (No. 5442PD210001).

W. Zhang (corresponding author), W. Sheng, and Q. Duan are with the Beijing Key Laboratory of Distribution Transform, China Electric Power Research Institute, Beijing 100192, China, and W. Zhang is also with the School of Electrical and Electronic Engineering, North China Electric Power University, Baoding, China (e-mail: crd-dk@163. com; wxsheng@epri. sgcc. com. cn; duanqing@epri.sgcc.com.cn).

H. Huang is with the State Key Laboratory of Alternate Electrical Power System with Renewable Energy Sources, North China Electric Power University, Beijing, China (e-mail: hhy4226@163.com).

X. Yan is with the School of Electrical and Electronic Engineering, North China Electric Power University, Baoding, China (e-mail: xiangwuy@163.com).

DOI: 10.35833/MPCE.2020.000921

	line l
N_G, N_R, N_B, N_{DS}	Numbers of generators, RESs, buses, and dispatchable sources
P_{Dkt}, P_{Dkt}^{fore}	Actual and forecasting power of demand k at time t
P_{DSit}	Actual generation of dispatchable source i at time t
$P_{DSit}^{\max}$, $P_{DSit}^{\min}$	The maximum and minimum outputs of dispatchable source i at time t
P_{Git}	Actual generation of SG i at time t
P_l, $P_l^{\max}$	Power flow and transmission capacity of line l
P_{Rj}^{MPPT}, P_{Rj}^{ref}	The maximum power point and power reference of RES j
P_{Rjt}, P_{Rjt}^{fore}	Actual and forecasting outputs of RES j at time t
P_{VSRjt}^{down}, $P_{VSRj}^{\min}$	Downward reserves and the minimum output of VSR j
P_{VSRjt}, P_{VSRjt}^{base}	Actual and base generation of VSR j at time t
P_{VSRjt}^{VUL}	Virtual upper limit for dispatchable portion of RES j at time t
P_{VSRjt}^{upward}, P_{VSRj}^{head}	Upward reserves and regulation headroom of VSR j
r_R	Percentage of standard deviation relative to forecasting value of RES
RR_i^{up}, RR_i^{down}	Upward and downward ramping limits of dispatchable source i
T_r	Length of reserve response time
T	Number of time slots
ΔT	Length of one schedule interval
u_i, d_i	Cost coefficients of upward and downward reserves
C. Variables	
β_{it}	Participation factor of dispatchable source i at time t
P_{DSit}^{base}	Base output of dispatchable source i at time t
P_{Git}^{base}	Base output of SG i at time t
r_{ait}^U, r_{ait}^D	Upward and downward reserves for RES and load provided by dispatchable source i at time t
r_{mit}^U, r_{mit}^D	Upward and downward contingency reserves provided by dispatchable source i at time t
$\boldsymbol{z}_D^+$, $\boldsymbol{z}_D^-$	Positive and negative slack row vectors for demand
z_{Dk}^+, z_{Dk}^-	Positive and negative slack variables for demand k
$\boldsymbol{z}_R^+$, $\boldsymbol{z}_R^-$	Positive and negative slack row vectors for RESs
z_{Rj}^+, z_{Rj}^-	Positive and negative slack variables for RES j

I. Introduction

DRIVEN by the energy crisis, sustainable development, and climate change, the renewable energy sources (RESs) represented by utility-scale wind power and solar energy have been widely utilized [1]. Since 2015, the market share of wind and solar power has increased from 4.6% to 9.8%, and consequently the market share of coal has decreased from 37.9% to 33% [2], which indicates that the coal power has been gradually displaced by the wind and solar power. China has formulated a clear path of renewable energy development and will manage to achieve carbon neutrality in 2060 [3]. Therefore, it is foreseeable that the wind and solar power will become the main power supply of the power generation mix in the future. As wind turbines and photovoltaic (PV) panels have low energy densies and are commonly integrated into the power grid through inverters, future power systems are characterized by high penetration of RESs and converter-dominated systems [4], [5].

The high-proportion inverter-based generation will deteriorates the frequency stability of power system. In traditional power systems, the power supply is made up of tens of or hundreds of synchronous generators (SGs), which possess frequency response capabilities and can be dispatchable on a long-term time scale. SGs provide the inertial response (IR), primary frequency response (PFR), and secondary frequency response (SFR), restoring the power balance and nominal frequency [6]. Especially, the automatic generation control (AGC) is tuned to maintain the nominal frequency, minimize the fuel cost, and avoid the undesirable conditions. In contrast to traditional SGs, RESs are commonly designed to exploit the maximum available generation and feed electricity into power grids passively, which are undispatchable and irresponsible from the view of system operators. Also, the output uncertainty of RES increases the degree of power imbalance. With the increasing penetration of RESs, the execution of AGC becomes more difficult with the remaining SGs, resulting in the maximum penetration limit of RES [7].

It is noted that the fundamental discrepancy between RESs and SGs is the capability of providing frequency responses and the dispatchability in the domain of frequency stability. Therefore, the concept and control strategies of virtual synchronous generator (VSG) are prompted to incorporate asynchronous RESs into the frame of active power and frequency control [8]-[13]. For practical energy sources, the emulation of IR and PFR can be realized by the "hidden inertia" for wind turbines, storage, and deloading strategy [14]. The deloading strategy deloads a controllable portion and make the RESs operate at the sub-optimal power point to keep the output margins. Compared with the approaches based on the "hidden inertia" and storage, the deloading strategy also enables RESs to adjust the output and keep headroom on mid- and long-term time scales [15]. Hence, the deloaded RESs can be treated as virtual synchronous renewables (VSRs) that are potential to participate in AGC.

On the formulation of the economic dispatch model, endogenous approaches are gaining popularity [16]-[25]. Based on the accurate knowledge of uncertain parameters, the stochastic optimization (SO) characterizes the uncertainties by establishing the scenarios causing high computation burden when multiple uncertainties are considered [16]. While the robust optimization (RO) only requires the knowledge of the range of uncertain parameters, it ignores the probability of a particular realization of uncertainties within the given range [17]. Therefore, RO has a better computation performance

but is more conservative. The conservatism of RO can be mitigated by the budget of the uncertainty, while the computation burden of SO can be mitigated by a scenario reduction technique [18], [19]. Furthermore, the Benders decomposition can be implemented to improve the computation performance of both SO and RO [20], [21].

In the economic dispatch model considering AGC, the participation factors are employed to determine the allocation of generation adjustment once the variation of renewable generation is revealed [16]. To deal with multiple uncertainties, the closely-related generation and reserves can be jointly scheduled to satisfy a series of operation and security constraints [22]. The reserves can be classified into two categories, including reserves coping with the uncertainties of RES and load (referred to as reserves for RES and load) as well as reserves coping with the N–1 faults (referred to as contingency reserves) [23], [24]. For power systems with the integration of RESs, the objective can be the operating cost considering the consumption of fossil fuels [25]. However, RESs are commonly treated as stochastic sources in the maximum power point tracking (MPPT) mode [16], [25], which means the dispatchable SGs provide all the adjustable responses.

As the inverter interfaces provide RESs with fast and accurate control capabilities, the optimal power flow is investigated based on practical control strategies of wind power [26]. The cap control enforces an absolute cap on the wind production to prevent excessive generation or reduce variability. However, if the RESs are treated as both power sources and reserve providers, the cap control may lead to ineffective use of the output capability. Based on the same concept of the deloading strategy, ΔP control monitors the maximum available wind power and keeps a controllable regulation headroom. However, this may cause a control latency and instability as the available regulation headroom varies continuously. In [27], the computed participation factors are proposed to be used as a lookup table for the system operation, but this also leads to the latency in AGC execution. In [28], the load model is comprised of uncontrollable and controllable portions. The uncontrollable portion is assumed known and constant, while the controllable portion is scheduled jointly with the generators. Therefore, the uncertain parameters of the demand are decomposed. In [17], an improved interval unit commitment (IIUC) formulation is proposed. The most probable predicted net load and its upper and lower bounds can form three non-probabilistic scenarios, and the ramp-up and ramp-down requirements are observed based on the highest slop. The IIUC provides another solution to investigate the characteristics of the uncertain parameters. Other approaches utilize storage systems such as utility-scale energy storage and pumped-storage hydropower plants to enhance the power balance regulation [25], [29].

In this paper, we focus on incorporating VSRs into active power and frequency control. Based on the concept of VSR and RO, a security-constrained economic dispatch (SCED) model is proposed to schedule the generation and reserves jointly. The contributions of this paper are as follows.

1) Based on the interval representation of uncertainties, the output of RES is transformed into a combination of a dispatchable portion with the virtual upper limit (VUL) and a stochastic portion with the original uncertainty. After the transformation, the RESs can be scheduled within the dispatchable portion. Also, there is no curtailment before the scheduling.

2) The control loops of determining the output reference of RESs in the VSR mode are designed. As the dispatchable portion provides guaranteed regulation capabilities between the VUL and the lower output limit, the base generation and upward reserves of VSRs are deterministic regarless of how the uncertainty of RES reveals. The permanent curtailment of RESs is analyzed, and the utilization and penetration of the generation capacity are derived.

3) Focusing on AGC, a new formulation of a robust SCED model is proposed, where the sources of power systems are divided according to their dispatchability. The dispatchable sources include the VSRs and SGs, while the undispatchable sources include the stochastic portion of the RESs. The case studies on 6-bus and 39-bus systems verify the correctness and effectiveness of the VSR mode compared with the MPPT mode.

The rest of this paper is organized as follows. Section II introduces the necessity of RESs participating in AGC and control strategy of VSR. Section III describes the formulation of the SCED model. Section IV introduces the solution strategy of handling nonlinear constraints. Section V discusses the case studies. Finally, Section VI concludes this paper.

II. Necessity of RESs Participating in AGC and Control Strategy of VSR

A. Necessity of RESs Participating in AGC

In the normal operation, the power systems are continually subjected to the disturbances caused by the uncertainties from the generation and load sides. In traditional power systems, the active power control and frequency control are multiple temporal stages of power balance and frequency regulation. When a persistent power deficiency or surplus causes the frequency to deviate for more than a predetermined duration, the SFR activates and restores the frequency to the nominal value by regulating the output of SGs selected by system operators, also known as AGC [6]. In the process of AGC in a single synchronous area, the area control error (ACE) representing the total required adjustment is firstly calculated. Then, the ACE is integrated, and the regional generation control signal is acquired. Finally, the selected SGs share the generation adjustment according to the participation factors.

The SGs and RESs vary greatly in the generation profiles and output characteristics. First, the outputs of wind and solar power are fluctuant and stochastic, primarily determined by instant meteorological conditions. The large-scale integration of RESs brings new uncertainty to the generation side and aggravates the worst imbalance scenario. Second, the wind and solar generation are designed to exploit the maximum available power. The RESs do not respond to frequency deviations, and the power electronic interfaces decouple

the physical connection between the RESs and the power grid. Therefore, with the increasing penetration of RESs and the consequent displacement of traditional SGs, the frequency stability of synchronous power systems deteriorates. Focusing on the SFR stage, multiple SGs are selected to satisfy the required regulation capacity and speed of AGC from the technical and economic perspective, and the power flow limits of transmission lines are also considered. When the regulation capability of the selected SGs is depleted, other SGs activate. However, the dynamic SFR capability is limited by the generation limits and the ramp rate. For example, the maximum continuous rating of SGs is typically 2% per minute [6]. As the current power systems are evolving towards 100% renewable energy generation [30], the participation of RESs in AGC should be considered necessary.

B. Control Strategy of VSR

The wind and solar power sources are also classified into inverter-based generation due to their asynchronous characteristics requiring inverter interfaces [31]. As the inverters have fast, accurate, and flexible regulation capability, the control strategies of inverter can be customized [32]. Generally, the layout of control diagram comprises a supplementary controller and a double-loop controller [33]. The double-loop controller ensures the accurate following of the control references, and the outer characteristics are largely determined by the supplementary controller [34]. In the transmission lines, the requivement of $X \gg R$ can be satisfied. By designing the controllers in the frequency domain and considering the short-current ratio (SCR) requirement on the integration of RESs, the decoupling of the active and reactive power control loops is always satisfied [35]. Therefore, by incorporating the characteristics of frequency control and ramping into the active power loops, the emulation of the outer characteristics of thermal SGs is realized [36]. Through the concept of VSR, RESs can be considered as traditional power plants, which enables them to participate in AGC. The deloading strategy makes the RESs operate at a sub-optimal power point below the maximum power point to keep the headroom used as regulation reserves [37]. The SFR is essentially an active power response that counteracts frequency deviations, reflecting the active power balance between the generation and demand. It is noted that the concepts of the maximum power point, sub-optimal power point, and regulation headroom are compatible with the generation limit, base generation point, and upward reserves. Therefore, the next step is to ensure that RESs can provide this regulation capability deterministically and continuously.

III. Formulation of SCED Model

A. Modeling of Uncertainty

In the RO, the output of RESs and load demand can be modeled by a nominal power and a power deviation limited by a given uncertainty set, which is expressed as:

$$\begin{cases} P_{Rjt} = P_{Rjt}^{fore} + \varepsilon_{Rjt} \\ P_{Dkt} = P_{Dkt}^{fore} + \varepsilon_{Dkt} \end{cases} \tag{1}$$

To eliminate the impact of different representations, we model the variable representing the output of RESs using the Gaussian probability density function [24]. For the demand, the uncertainty is usually treated as a Gaussian distribution random variable [16]. Based on the characteristics of Gaussian distribution, the standard deviation σ_{Rjt} of RES j is defined as:

$$\sigma_{Rjt} = r_R P_{Rjt}^{fore} \tag{2}$$

For RES j, we have $\varepsilon_{Rjt} \in (-\zeta_{Rjt}, \zeta_{Rjt})$ and the upper and lower bounds of the uncertainty set can be defined as:

$$\begin{cases} \zeta_{Rjt} = 3\sigma_{Rjt} \\ -\zeta_{Rjt} = -3\sigma_{Rjt} \end{cases} \tag{3}$$

The uncertainty set $(-\zeta_{Rjt}, \zeta_{Rjt})$ covers 99.74% quantile of the output of RES. In the same way, the uncertain parameter of the demand k can be modeled by a forecasting power P_{Dkt}^{fore} with an uncertainty set $(-\zeta_{Dkt}, \zeta_{Dkt})$ and we have $\varepsilon_{Dkt} \in (\zeta_{Dkt}, \zeta_{Dkt})$.

B. Transformation of RES Output

Based on the forecasting generation and uncertainty set, the output of RES can be transformed into dispatchable and stochastic portions.

The dispatchable portion is restricted by a VUL in (4), which indicates the maximum guaranteed output of RES regardless of how its uncertainty realizes.

$$P_{VSRjt}^{VUL} = P_{Rjt}^{fore} - \zeta_{Rjt} \tag{4}$$

The stochastic portion η_{Rjt} is a Gaussian uncertainty variable, which inherits the original stochastic characteristics. The expected generation of η_{Rjt} is ζ_{Rjt}.

The synthesis of the two portions is given by:

$$P_{Rjt} = (P_{Rjt}^{fore} - \zeta_{Rjt}) + \eta_{Rjt} = P_{VSRjt}^{VUL} + \eta_{Rjt} \tag{5}$$

It is noted that the synthesis of the RES output is still stochastic. Based on the transformation, there is no curtailment before solving the SCED model, and the original uncertainty remains the same. The dispatchable and stochastic portions of the RES output is shown in Fig. 1. The margin between the VUL and the base generation of VSR functions as the headroom of frequency responses.

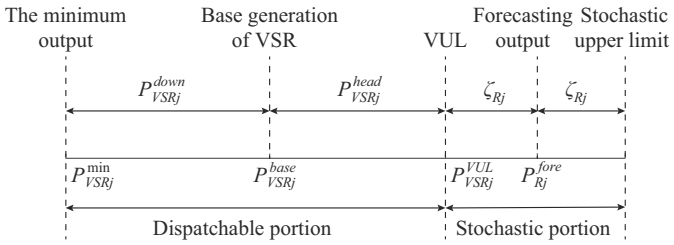

Fig. 1. Dispatchable and stochastic portions of RES output.

The stochastic portion can be treated as a stochastic source, of which the output is represented as:

$$\eta_{Rjt} = \zeta_{Rjt} + \varepsilon'_{Rjt} \tag{6}$$

From Fig. 1, the power deviation ε'_{Rj} can be limited by the uncertainty set $(-\zeta_{Rjt}, \zeta_{Rjt})$, i.e., $\varepsilon'_{Rj} \in (-\zeta_{Rj}, \zeta_{Rj})$.

C. Control Design and Analysis

The renewable energy prediction provides available forecasting power in each time interval, and the MPPT strategy tracks the available power in real time, which is realized within the dispatchable portion.

In the MPPT or VSR mode with no reserved headroom, the output of RESs can be represented as the combination of the whole dispatchable portion and the stochastic portion as:

$$P_{VSRj}^{VUL}+\eta_{Rj}=P_{Rj}^{MPPT} \tag{7}$$

In the dispatchable portion, if the upward reserves are scheduled, the headroom between the base generation and the VUL provides this regulation capability, which can be expressed as:

$$P_{VSRj}^{base}+P_{VSRj}^{head}=P_{VSRj}^{VUL} \tag{8}$$

It is noted that the upward reserves may not fully utilize the capability of the regulation headroom. The scheduled base generation of dispatchable sources satisfies the power balance between generation and demand, while the continuous and discrete uncertainties largely influence the scheduled reserves, so we have:

$$P_{VSRj}^{upward}\le P_{VSRj}^{head} \tag{9}$$

Equation (10) can be encoded by the limit constraints of generation capacity considering the upward reserves. Combined with the stochastic portion, the expected output of RES is expressed as:

$$P_{VSRj}^{base}+\eta_{Rj}=P_{Rj}^{MPPT}-P_{VSRj}^{head} \tag{10}$$

Based on (10), the power reference of RES, i.e., the reference of sub-optimal power point, is given by:

$$P_{Rj}^{ref}=P_{Rj}^{MPPT}-P_{VSRj}^{head} \tag{11}$$

The control loops of determining the power reference of RESs are accordingly designed and shown in Fig. 2. It is noted that VSR mode is based on the same concept with the deloading strategy and ΔP control, but the realization and tracking of the maximum power point do not influence the availability of the regulation headroom.

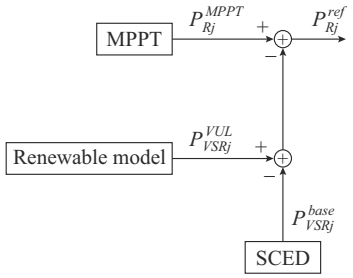

Fig. 2. Control loops of determining power reference of RESs.

From Fig. 2 and (11), it is concluded that the regulation headroom causes permanent curtailment. We define the utilization percentage $u_{percent}$ to evaluate the expected efficiency in VSR mode, which is expressed as:

$$u_{percent}=1-\frac{\sum_{j=1}^{N_R}P_{VSRj}^{head}}{\sum_{j=1}^{N_R}P_{Rj}^{fore}} \tag{12}$$

Similarly, the expected penetration level of RES r_{pene} is defined as:

$$r_{pene}=\frac{\sum_{j=1}^{N_R}(P_{Rj}^{fore}-P_{VSRj}^{head})}{\sum_{k=1}^{N_B}P_{Dk}^{fore}} \tag{13}$$

D. Incorporating VSR into SCED

When taking RESs as undispatchable sources, the conventional formulation of the joint scheduling of generation and reserves has been well addressed such as the affinely adjustable robust optimal power flow in [16] and the endogenous approach proposed in [24]. As the time scale of AGC is from 30 s to 15 min, which is much shorter than the start-up and shut-down time of SGs, we only consider spinning reserves [38], [39]. Based on the output transformation, VSRs are also dispatchable. Therefore, the SGs and VSRs are combined as dispatchable sources. When executing AGC, the output of dispatchable sources is expressed as:

$$P_{DSit}=P_{DSit}^{base}-\beta_{it}\left(\sum_{j=1}^{N_R}\varepsilon'_{Rjt}-\sum_{k=1}^{N_B}\varepsilon_{Dkt}\right)\quad i=1,2,...,N_{DS} \tag{14}$$

where $N_{DS}=N_G+N_R$.

In (14), the stochastic portion of RESs is considered as separated stochastic sources. It is noted that VSRs have two merits: ① the generation cost is assumed to be zero as they do not consume fossil fuels [24], [25]; ② the control of inverters is extremely fast and accurate compared with SGs, and the ramp rate of inverter-interfaced VSRs is much larger than that of SGs [31].

The operating cost is comprised of generation and reserve costs. The generation cost can be represented as a quadratic cost function, while the reserve cost can be represented as a linear function. The optimization goal of the proposed SCED model is to minimize the overall operating cost:

$$\min\sum_{t=1}^{T}\left\{\sum_{i=1}^{N_G}[a_i(P_{Git}^{base})^2+b_iP_{Git}^{base}+c_i]+\sum_{i=1}^{N_{DS}}[u_i(r_{ait}^{U}+r_{mit}^{U})+d_i(r_{ait}^{D}+r_{mit}^{D})]\right\} \tag{15}$$

Equation (15) is subjected to the following constraints.

1) Constraint for forecasting power balance

$$\sum_{i=1}^{N_{DS}}P_{DSit}^{base}+\sum_{j=1}^{N_R}\eta_{Rjt}^{fore}=\sum_{k=1}^{N_B}P_{Dkt}^{fore}\quad\forall t \tag{16}$$

Constraint (16) states that the power balance should be satisfied before the realization of uncertainties.

2) Constraint for generation capacity limit

$$P_{DSit}^{\min}\le P_{DSit}\le P_{DSit}^{\max}\quad\forall i,\forall t \tag{17}$$

Constraint (17) states that the output of the dispatchable source i should not exceed the upper and lower limits. It is noted that for SGs, the minimum and maximum limits are constant, while for VSRs, the maximum limits are the VULs and fluctuant in different time intervals.

3) Constraint for line capacity limit

$$\left|\sum_n L_{ln}\left(\sum_i I_{ni}^1 P_{DSit}+\sum_j I_{nj}^2 \eta_{Rjt}-\sum_k I_{nk}^3 P_{Dkt}\right)\right| \le P_l^{\max} \quad \forall t \tag{18}$$

Constraint (18) states that the power flow of transmission lines should not exceed the bidirectional capacity limits.

4) Constraint for ramp limit of SGs

$$-RR_i^{down}\Delta T \le P_{Gi(t+1)}^{base}-P_{Git}^{base} \le RR_i^{up}\cdot\Delta T \quad t=1,2,...,T-1, \forall i \in N_G \tag{19}$$

Constraint (19) states that the variation of generator i is limited by the ramp rate over any two consecutive time slots.

5) Constraints for ramp limits of reserves

$$r_{ait}^U + r_{mit}^U \le RR_i^{up}\cdot T_r \quad \forall i \in N_G, \forall t \tag{20}$$

$$r_{ait}^D + r_{mit}^D \le RR_i^{down}\cdot T_r \quad \forall i \in N_G, \forall t \tag{21}$$

Constraints (20) and (21) state that the provision of upward and downward reserves is limited by the ramp rate within the reserve response time.

6) Constraints for generation capacity limit considering reserves

$$P_{DSit}^{\min} \le P_{DSit}^{base}-(r_{ait}^D+r_{mit}^D) \quad \forall i, \forall t \tag{22}$$

$$P_{DSit}^{base}+r_{ait}^U+r_{mit}^U \le P_{DSit}^{\max} \quad \forall i, \forall t \tag{23}$$

Constraints (22) and (23) state that the output of dispatchable source i is limited by the upper and lower limits considering both the base generation and the provision of upward and downward reserves, respectively.

7) Constraints for reserve requirement considering uncertainties of RES and demand

$$r_{ait}^U \ge \beta_{it}\left(\sum_{j=1}^{N_R}\zeta_{Rjt}+\sum_{k=1}^{N_B}\zeta_{Dkt}\right) \quad \forall i, \forall t \tag{24}$$

$$r_{ait}^D \ge \beta_{it}\left(\sum_{j=1}^{N_R}\zeta_{Rjt}+\sum_{k=1}^{N_B}\zeta_{Dkt}\right) \quad \forall i, \forall t \tag{25}$$

Constraints (24) and (25) state that the total scheduled upward and downward reserves dealing with the uncertainties of RES and demand should satisfy the requirements in the worst scenario.

8) Constraint for reserve requirement considering the $N-1$ criterion

$$\sum_{i=1,i\ne u}^{N_{DS}} r_{mit}^U \ge P_{DSut}^{base} \quad \forall u, \forall t \tag{26}$$

As the outage of two or more generators rarely happens, we only consider the $N-1$ criterion [25]. Constraint (26) states that the total upward contingency reserves should cover the loss of any single unit of the dispatchable sources.

9) Constraints for participation factor

$$\sum_i \beta_{it} = 1 \quad \forall t \tag{27}$$

$$0 \le \beta_{it} \le 1 \quad \forall i, \forall t \tag{28}$$

Constraints (27) and (28) state that the participation factors should be non-negative and sum to one.

IV. Model Solution

In order to solve the SCED model, the constraints should retain the linearity [16]. However, in (18), the power of the stochastic portion of the RESs and the demand are stochastic. Moveover, the output of dispatchable sources is also stochastic due to the response to the realization of uncertainties. Therefore, (17) and (18) are nonlinear and the relevant constraints need to be transformed into deterministic ones. As shown in (29) and (30), (17) and (18) are represented by matrices, respectively, and the subscript t is omitted for simplicity.

$$\boldsymbol{P}_{DS}^{\min} \le \boldsymbol{P}_{DS}^{base}-\boldsymbol{\beta}\mathbf{1}^1\boldsymbol{\varepsilon}_R'+\boldsymbol{\beta}\mathbf{1}^2\boldsymbol{\varepsilon}_D \le \boldsymbol{P}_{DS}^{\max} \tag{29}$$

$$-\boldsymbol{P}_L^{\max} \le \boldsymbol{L}[\boldsymbol{I}^1\boldsymbol{P}_{DS}+\boldsymbol{I}^2(\boldsymbol{\eta}_R^{fore}+\boldsymbol{\varepsilon}_R')-\boldsymbol{I}^3(\boldsymbol{P}_D^{fore}+\boldsymbol{\varepsilon}_D)] \le \boldsymbol{P}_L^{\max} \tag{30}$$

The matrices $\boldsymbol{A}$, $\boldsymbol{B}$, $\boldsymbol{C}$, and $\boldsymbol{d}$ are defined as:

$$\begin{cases} \boldsymbol{A}=[\boldsymbol{I} \quad \boldsymbol{I} \quad \boldsymbol{LI}^1 \quad -\boldsymbol{LI}^1]^{\mathrm{T}} \\ \boldsymbol{B}=[-\boldsymbol{\beta}\mathbf{1}^1 \quad \boldsymbol{\beta}\mathbf{1}^1 \quad -\boldsymbol{LI}^1\boldsymbol{\beta}\mathbf{1}^1+\boldsymbol{LI}^2 \quad \boldsymbol{LI}^1\boldsymbol{\beta}\mathbf{1}^1-\boldsymbol{LI}^2]^{\mathrm{T}} \\ \boldsymbol{C}=[\boldsymbol{\beta}\mathbf{1}^2 \quad -\boldsymbol{\beta}\mathbf{1}^2 \quad \boldsymbol{LI}^1\boldsymbol{\beta}\mathbf{1}^2-\boldsymbol{LI}^3 \quad -\boldsymbol{LI}^1\boldsymbol{\beta}\mathbf{1}^2+\boldsymbol{LI}^3]^{\mathrm{T}} \\ \boldsymbol{d}=[\boldsymbol{P}_{DS}^{\max} \quad -\boldsymbol{P}_{DS}^{\min} \quad \boldsymbol{P}_L^{\max}-\boldsymbol{LI}^2\boldsymbol{\eta}_R^{fore}+\boldsymbol{LI}^3\boldsymbol{P}_D^{fore} \quad \boldsymbol{P}_L^{\max}+ \\ \qquad \boldsymbol{LI}^2\boldsymbol{\eta}_R^{fore}-\boldsymbol{LI}^3\boldsymbol{P}_D^{fore}]^{\mathrm{T}} \end{cases} \tag{31}$$

Therefore, (29) and (30) can be expressed as:

$$\boldsymbol{A}\boldsymbol{P}_{DS}^{base}+\boldsymbol{B}\boldsymbol{\varepsilon}_R'+\boldsymbol{C}\boldsymbol{\varepsilon}_D \le \boldsymbol{d} \tag{32}$$

The RO seeks to find the optimal solutions for all possible realization of uncertainties within prescribed intervals. For the m^{th} row of (32), (33) is satisfied

$$\boldsymbol{A}_m\boldsymbol{P}_{DS}^{base}-\boldsymbol{d}_m+\max(\boldsymbol{B}_m\boldsymbol{\varepsilon}_R')+\max(\boldsymbol{C}_m\boldsymbol{\varepsilon}_D) \le \boldsymbol{0} \tag{33}$$

By making use of slack row vectors $\boldsymbol{z}_R^+/\boldsymbol{z}_R^-$, $\max(\boldsymbol{B}_m\boldsymbol{\varepsilon}_R')$ can be expressed as:

$$\sum_{B_{mj}\ge 0} B_{mj}\zeta_{Rj}+\sum_{B_{mj}<0} B_{mj}(-\zeta_{Rj}) \le \boldsymbol{z}_R^+\boldsymbol{\zeta}_R+\boldsymbol{z}_R^-(-\boldsymbol{\zeta}_R) \tag{34}$$

where the elements in the slack row vector $\boldsymbol{z}_R^+/\boldsymbol{z}_R^-$ satisfy $z_{Rj}^+ \ge 0$, $z_{Rj}^+ \ge B_{mj}$, $z_{Rj}^- \le 0$, and $z_{Rj}^- \le B_{mj}$; and $\boldsymbol{\zeta}_R$ is the column vector comprising the maximum variations of the stochastic portion of RESs.

In the same way, $\max(\boldsymbol{C}_m\boldsymbol{\varepsilon}_D)$ can be expressed as:

$$\sum_{C_{mk}\ge 0}^{N_B} C_{mk}\zeta_{Dk}+\sum_{C_{mk}\le 0}^{N_B} C_{mk}(-\zeta_{Dk}) \le \boldsymbol{z}_D^+\boldsymbol{\zeta}_D+\boldsymbol{z}_D^-(-\boldsymbol{\zeta}_D) \tag{35}$$

where the elements in the slack row vector $\boldsymbol{z}_D^+/\boldsymbol{z}_D^-$ satisfy $z_{Dk}^+ \ge 0$, $z_{Dk}^+ \ge C_{mk}$, $z_{Dk}^- \le 0$, and $z_{Dk}^- \le C_{mk}$; and $\boldsymbol{\zeta}_D$ is the column vector comprising the maximum variations of the demand.

From (34) and (35), the linearity of the constraints is ensured. Then, the SCED model can be solved by mixed-integer programming.

V. Case Analysis

To verify the validity of the proposed model, we carry out case analysis on 6-bus and 39-bus systems and perform the SCED model for 16 periods representing the solar fluctuations in one day. The generation and load are based on historical data of State Grid Corporation of China. Four typical days are selected to represent four seasons in one year. The conventional SCED model, in which the solar generation op-

erates in the MPPT mode, is also solved as a comparison. The formulation of SCED model is programmed in MATLAB and solved using Gurobi, and the test environment is Intel i7 3.6 GHz with 16 GB of memory.

A. 6-bus System

The parameters of generators and lines in the 6-bus system are shown in [40]. A solar plant is connected at bus 2. From scenario 1 to scenario 8, the solar generation grows at 10% in each step, indicating the increasing installed capacity, while the demand remains the same in these scenarios. The forecasting solar generation in scenario 1 and load demand in the 6-bus system are shown in Fig. 3. We assume that the solar generation and load demand are Gaussian distribution random variables with standard deviations $\sigma_{Rj}=0.05P_{Rj}^{fore}$ and $\sigma_{Dk}=0.01P_{Dk}^{fore}$, respectively. It should be mentioned that, in practice, ζ_{Rj} and ζ_{Dk} can use the confidence interval of forecasting error provided by the prediction method in [41]. We assume the reserve cost coefficients of the VSR to be the mean value of those of the SGs.

To verify the robustness and superiority of the proposed approach, the comparisons are carried out between the VSR mode and MPPT mode.

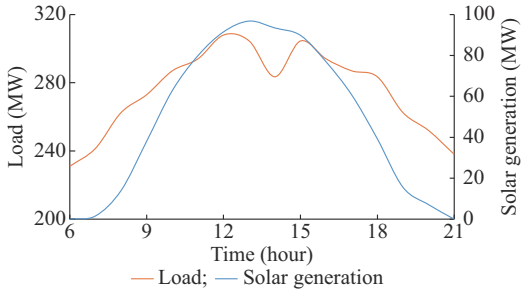

Fig. 3. Forecasting solar generation in scenario 1 and load demand in 6-bus system.

In the MPPT mode, the SCED model is infeasible when the forecasting solar generation increases to the level of scenario 4, whereas the VSR mode is feasible in all scenarios.

The scheduled generation and reserves in the VSR mode in the 6-bus system are shown in Fig. 4, where the forecasting value of solar generation and the base output of VSR are denoted as "Forecasts" and "Base", respectively; the stochastic portion is denoted as "Stochastic"; the upward and downward reserves dealing with continuous reserves are denoted as "VSR-upward" and "VSR-downward", respectively; and the contingency reserve is denoted as "VSR-fault".

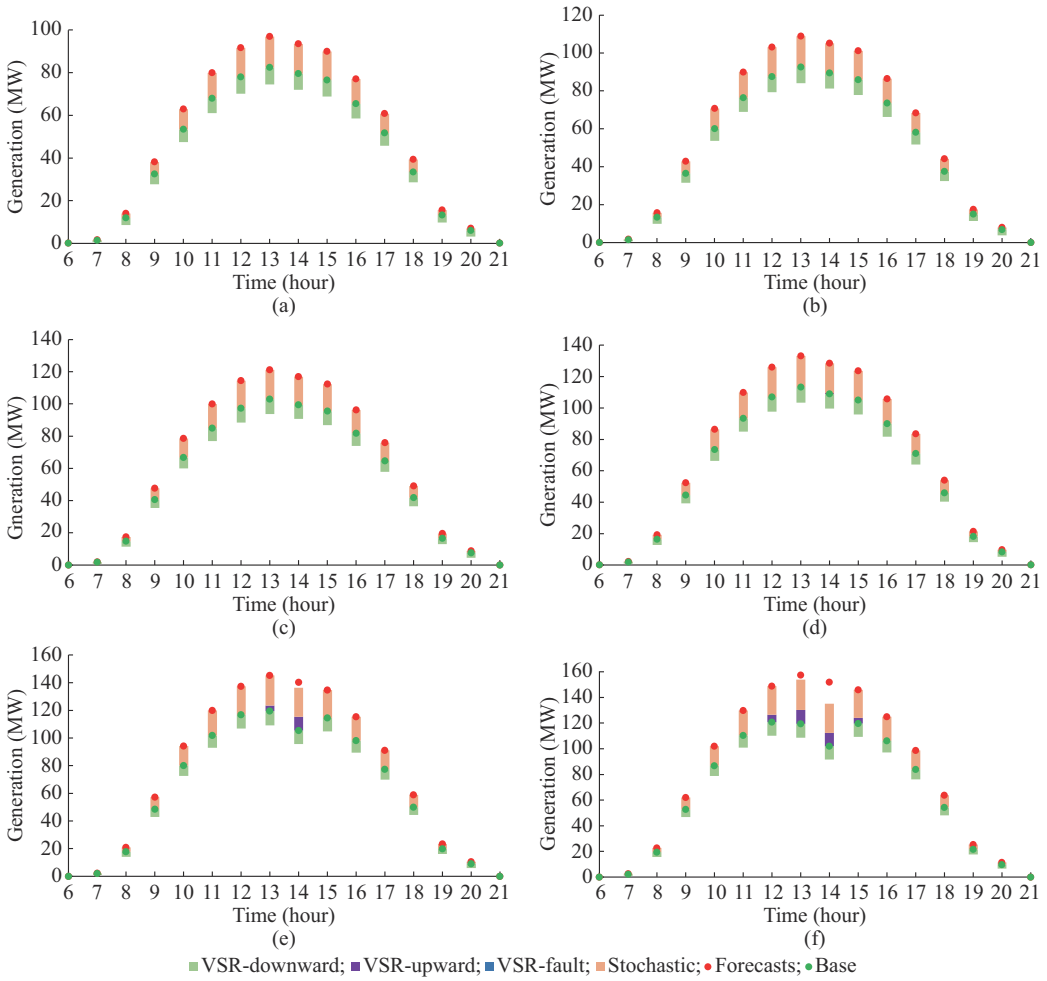

Fig. 4. Scheduled generation and reserves in VSR mode in 6-bus system. (a) Scenario 1. (b) Scenario 2. (c) Scenario 3. (d) Scenario 4. (e) Scenario 5. (f) Scenario 6.

In scenarios 1-3, the expectation of solar generation equals the forecasting value. This is because the solar plant does not need to curtail or keep headroom for the upward reserve provision. Therefore, the MPPT and VSR modes are both feasible. In scenarios 4-6, the expectation of solar generation is less than the forecasting value because of the headroom, which indicates the solar generation needs to be deloaded and provide upward reserves for the continuous uncertainties. In scenarios 5 and 6, the upward reserves do not fully utilize the headroom because of the lower limits of other SGs. Also, the VSR provides downward reserves for RES and load in all the scenarios. From the results, it can be concluded that the solar plant in the VSR mode can actively participate in the power balance regulation.

VSRs can actively curtail in case of excessive generation in scenarios 4-6, and the participation factors in the 6-bus system are shown in Fig. 5, where G1-G3 represent the SGs. The results show that the VSR participates in AGC jointly with the SGs when the solar generation reaches the peak by the early afternoon.

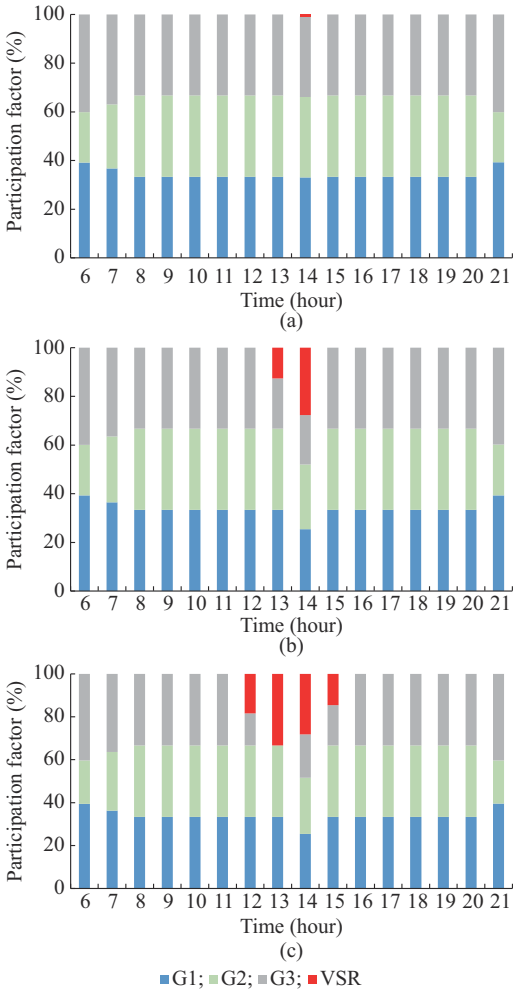

Fig. 5. Participation factors in VSR mode in 6-bus system. (a) Scenario 4. (b) Scenario 5. (c) Scenario 6.

The total operating costs of the MPPT and VSR modes in the 6-bus system are compared, as shown in Fig. 6. As the reserve cost coefficients of the VSR are defined as the mean value of those of other SGs, the VSR mode is slightly more economical than MPPT mode. The cost is further reduced since VSR mode is feasible in the cases of higher solar penetration levels.

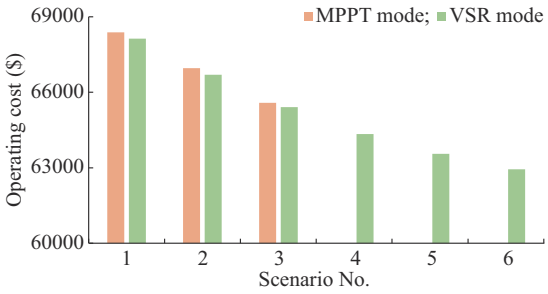

Fig. 6. Comparison of operating costs between MPPT and VSR modes in 6-bus system.

Considering four seasons in a whole year, the MPPT and VSR modes are both feasible in scenarios 1-3, and there is no curtailment or scheduled upward reserves in the VSR mode. Hence, the expectation of the utilization percentages of MPPT and VSR modes are equal. As the solar generation capability increases, only the VSR mode is feasible. The scheduled regulation headroom causes a permanent curtailment in spring and summer.

The utilization percentages of solar capacity in spring and summer in the 6-bus system are shown in Fig. 7. The curtailment is ascribed to the minimum output limits of the generators.

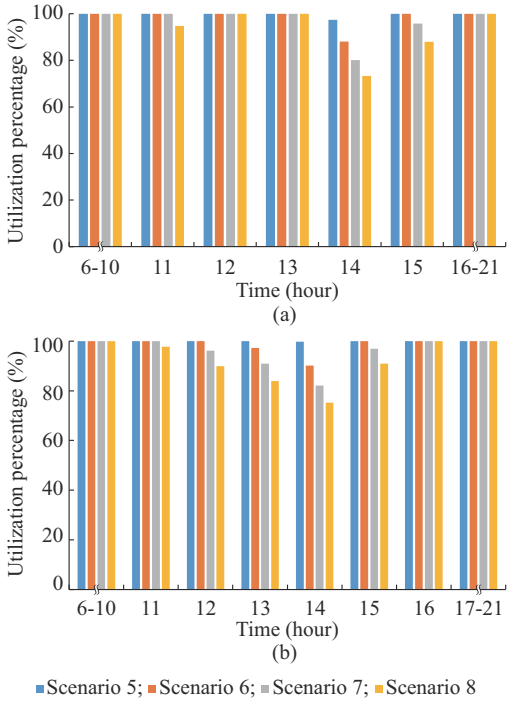

Fig. 7. Utilization percentages of solar capacity in different seasons in 6-bus system. (a) In spring. (b) In summer.

By summarizing the seasonal results, the annual curtailment and penetration levels of solar generation in the 6-bus system are shown in Fig. 8. The results show that both the

curtailment and penetration levels increase as the generation capacity increases. As the demand remains constant, the increasing solar penetration also reflects the displacement of SGs.

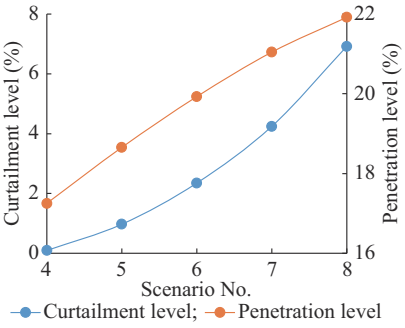

Fig. 8. Annual curtailment and penetration levels of solar generation in VSR mode in 6-bus system.

The forecasting error is an important factor influencing the renewable uncertainty. The SCED model is solved considering various standard deviations, including 0%, 1%, 3%, and 5% of the forecasting value. The operating costs and utilization percentages considering various forecasting errors in different scenarios in the 6-bus system are shown in Fig. 9. The results show that larger forecasting errors lead to more operating cost and solar curtailment.

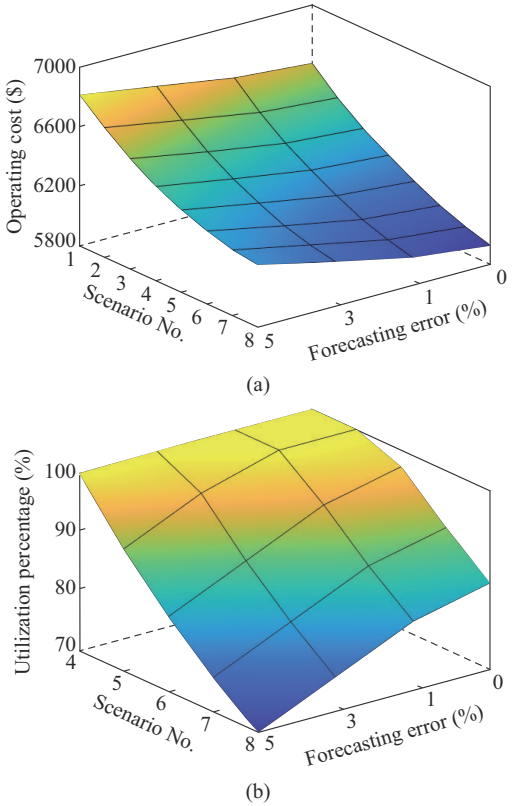

Fig. 9. Operating cost and utilization percentage considering various forecasting errors in 6-bus system. (a) Operating cost. (b) Utilization percentage.

B. 39-bus System

The parameters of generators and lines of the 39-bus system are shown in [25]. Solar plants are connected at buses 4, 8, 20, and 39. The remaining data are determined in the same way as those in the 6-bus case. The forecasting solar generation in scenario 1 and load demand in the 39-bus system are shown in Fig. 10.

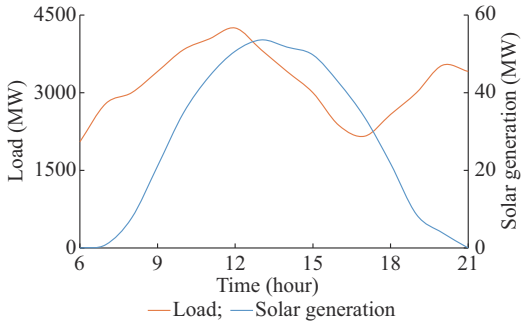

Fig. 10. Forecasting solar generation in scenario 1 and load demand in 39-bus system.

The scheduled generation and reserves in the VSR mode in the 39-bus system is shown in Fig. 11. The results are consistent with those in the 6-bus case. First, the solar capacity restricts the feasibility of MPPT mode, but the VSR mode is feasible in all scenarios. Second, the MPPT mode passively feeds power, but the VSR mode provides not only downward reserves but also upward reserves for solar generation and load at intervals with excessive solar generation. Third, the VSR mode curtails the solar power actively when providing upward reserves. In all the scenarios where the RESs provide the upward reserve, the headroom is fully utilized. From the results, it is concluded that the VSRs can participate in power balance regulation and AGC actively.

The participation factors of SGs (G1-G10) and VSRs (VSR1-VSR4) in scenarios 4-6 in the 39-bus system are shown in Fig. 12. As the demand is relatively low at 17:00, the solar plant is scheduled to balance the generation and demand.

The total costs of the MPPT and VSR modes in the 39-bus system are compared, as shown in Fig. 13. The VSR mode provides a feasible and economical solution as the solar generation capacity increases.

Considering the operation in a whole year, the VSR mode only causes the curtailment in spring and summer. The utilization percentages of solar capactity in spring and summer in the 39-bus system are shown in Fig. 14.

By summarizing the seasonal results, the annual curtailment and penetration levels of solar generation in the 39-bus system are shown in Fig. 15. The results show that the penetration and curtailment levels both increase as the solar capacity increases.

Considering various forecasting errors identified by standard deviations, including 0%, 1%, 3%, and 5%, the operating cost and utilization percentages in different scenarios are shown in Fig. 16. Compared with the case of 6-bus system, larger forecasting errors still lead to more operating costs and solar curtailment.

In conclusion, the VSR mode can increase the maximum penetration level of RESs, sustain security, and operation requirements, and decrease the operation cost.

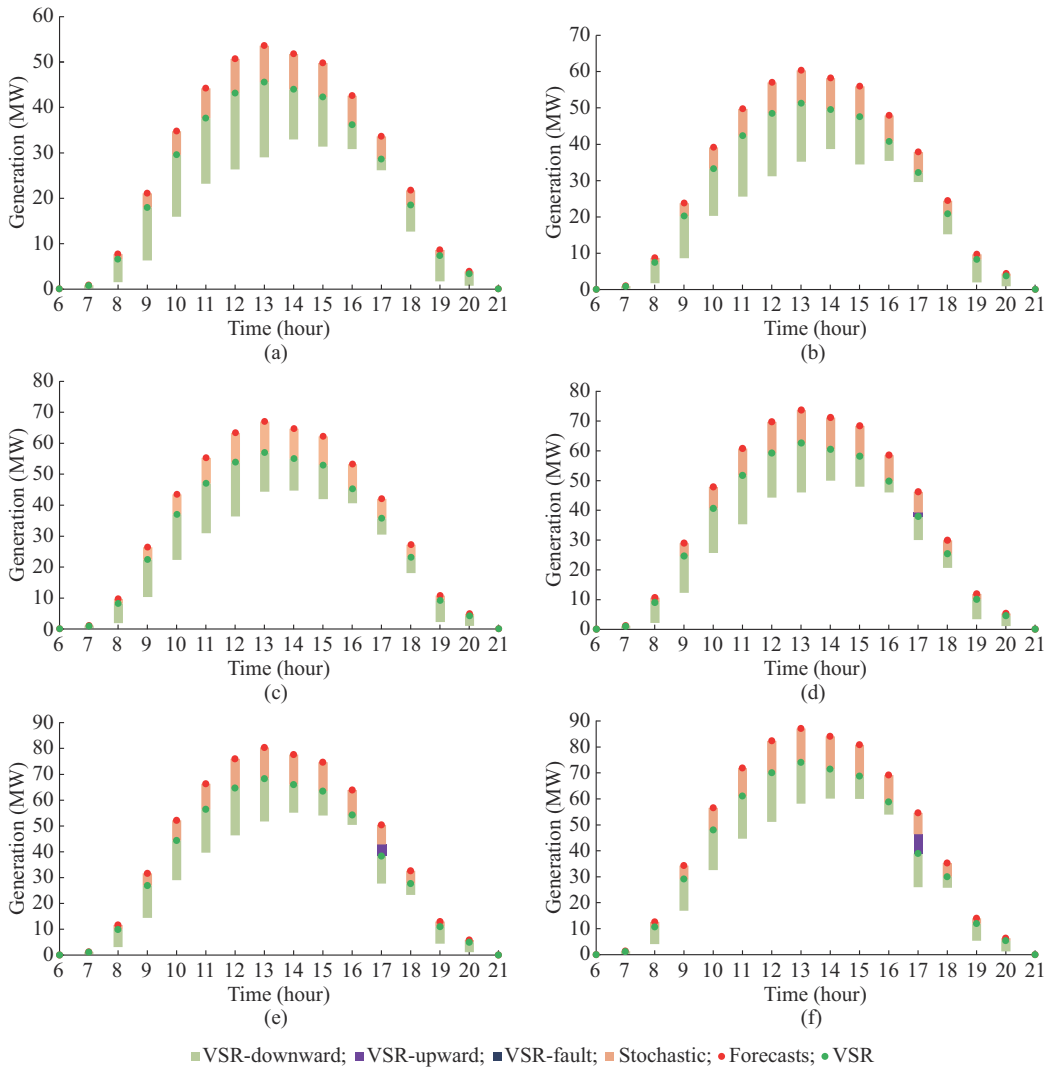

Fig. 11. Scheduled generation and reserves in VSR mode in 39-bus system. (a) Scenario 1. (b) Scenario 2. (c) Scenario 3. (d) Scenario 4. (e) Scenario 5. (f) Scenario 6.

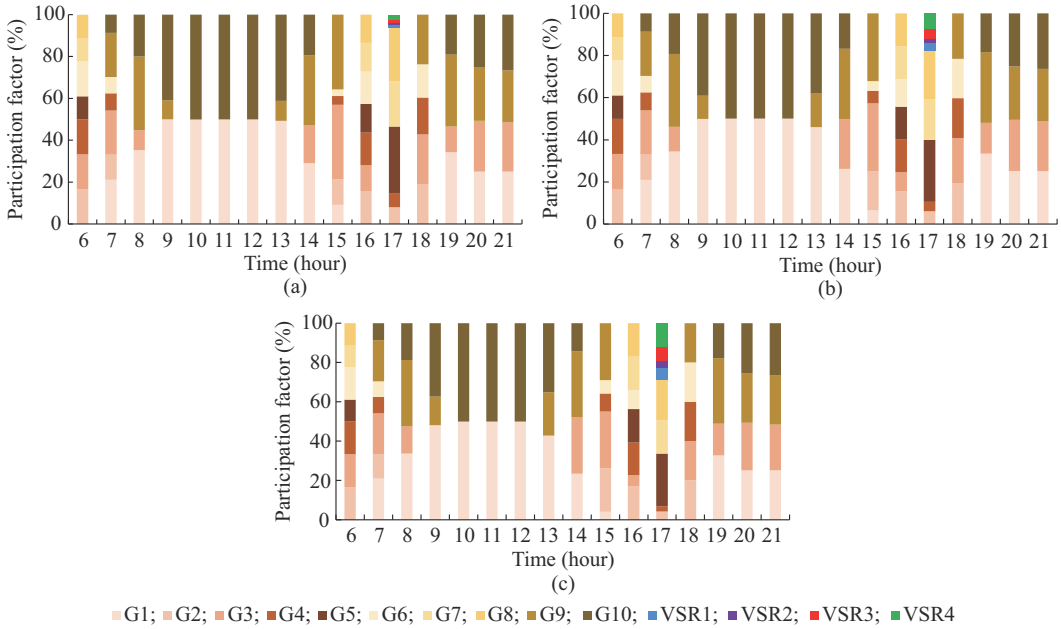

Fig. 12. Participation factors in VSR mode in 39-bus system.

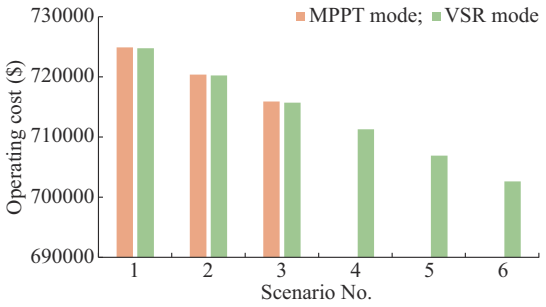

Fig. 13. Comparison of operating cost between MPPT and VSR modes in 39-bus system.

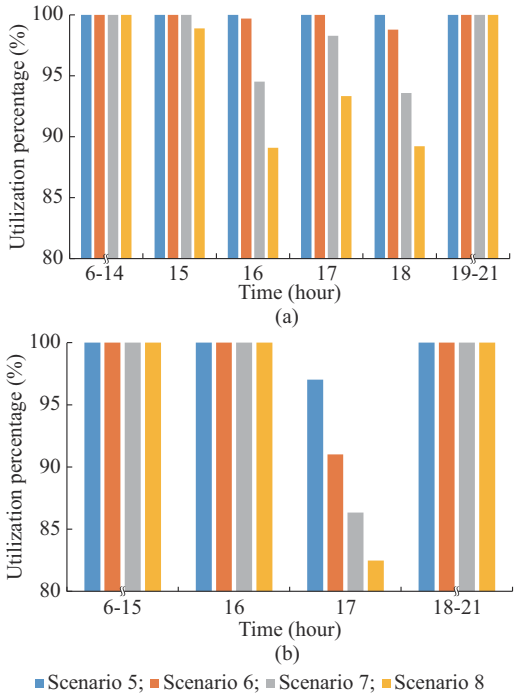

Fig. 14. Utilization percentages of capacity in different seasons in 39-bus system. (a) In spring. (b) In summer.

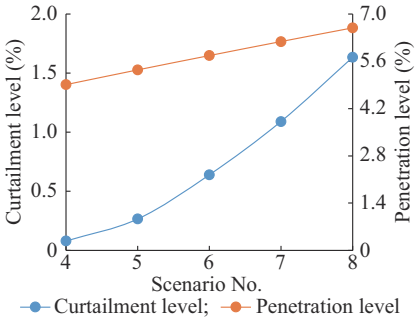

Fig. 15. Annual curtailment and penetration levels of solar generation in VSR mode in 39-bus system.

VI. Conclusion

To increase the AGC regulation resources in power systems with high penetration of inverter-interfaced RESs, an SCED model to realize the joint scheduling of generation and reserves is presented considering that RESs operate in VSR mode. The conclusions are summarizes as follows:

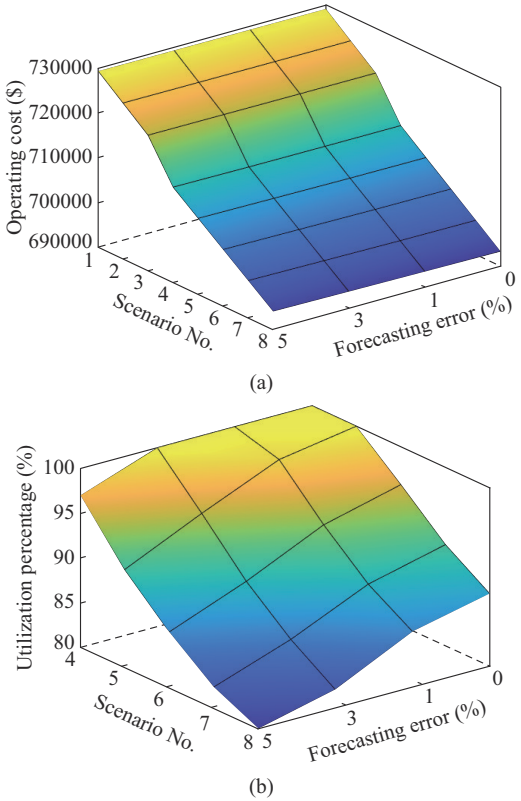

Fig. 16. Operating cost and utilization percentage considering various forecasting errors in 39-bus system. (a) Operating cost. (b) Utilization percentage.

1) Based on the interval representation of renewable uncertainty, the dispatchable portion of the RES output is decomposed. The permanent curtailment is ascribed to the headroom, which can provide upward reserves.

2) According to the realization of uncertainties, VSRs can participate in AGC jointly with SGs by providing the upward and downward reserves.

3) Compared with the MPPT mode, the VSR mode can increase the maximum penetration level of RESs and decrease the operating cost.

4) From the annual data, the penetration level increases with the growing renewable capacity, but the curtailment also increases under the assumption of constant load profiles.

5) The operating cost and renewable utilization are influenced by the forecasting accuracy of the renewable generation, so the reduction of forecasting errors is thus necessary. In conclusion, the VSR mode provides a new operation mode for sustaining the power balance and frequency stability.

As energy storage systems provide the flexibility, the unit commitment is another important topic, and the day-ahead scheduling considering the start-up and shut-down of SGs and flexible control of storage systems is in the scope of our future work.

References

[1] X. Yan and W. Zhang, "Review of VSG control-enabled universal compatibility architecture for future power systems with high-penetration renewable generation," *Applied Sciences*, vol. 9, no. 7, pp. 1453-

1472, Mar. 2019.
[2] Ember. (2020, Aug.). Wind and solar now generate one-tenth of global electricity global half-year electricity analysis. [Online]. Available: https://ember-climate. org/wp-ontent/uploads/2020/08/Report-Ember-Global-Electricity-Review-H1-2020.pdf
[3] CWEA. (2009, Apr.). Statistical brief of wind power lifting capacity in China in 2018. [Online]. Available: http://www.cwea.org.cn/news_latest_detail.html?id=217
[4] Z. Lu, Y. Ye, L. Guo *et al*., "Frequency regulation challenge of power electronics dominated power systems and its new multi-level coordinated control framework," *Electric Power*, vol. 52, no. 4, pp. 8-17, Aug. 2019.
[5] C. Kang and L. Yao, "Key scientific issues and theoretical research framework for power systems with high proportion of renewable energy," *Automation of Electric Power Systems*, vol. 41, no. 9, pp. 1-11, May 2017.
[6] P. Kundur, *Power System Stability and Control*. NewYork: McGrawHill, 1993, pp. 581-626.
[7] J. K. Kaldellis, "Evaluating the maximum wind energy penetration limit for weak electrical grids," in *Proceedings of 2001 European Wind Energy Conference and Exhibition*, Copenhagen, Denmark, Jul. 2001, pp. 1-6.
[8] H. P. Beck and R. Hesse, "Virtual synchronous machine," in *Proceedings of the 9th International Confeference Electrical Power Quality Utilisation*, Barcelona, Spain, Oct. 2007, pp. 1-6.
[9] Q. Zhong and G. Weiss, "Synchronverters: inverters that mimic synchronous generators," *IEEE Transactions on Industrial Electronics*, vol. 58, no. 4, pp. 1259-1267, Apr. 2011.
[10] Q. Zhong, "Virtual synchronous machines: a unified interface for grid integration," *IEEE Power Electronics Magazine*, vol. 3, no. 4, pp. 18-27, Dec. 2016.
[11] W. Zhang and X. Yan, "Equivalence analysis of virtual synchronous machines and frequency-droops for inertia emulation in power systems with converter-interfaced renewables," *Journal of Electrical Engineering & Technology*, vol. 15, pp. 1167-1175, Mar. 2020.
[12] K. Jiang, H. Su, and H. Lin *et al*., "A practical secondary frequency control strategy for virtual synchronous generator," *IEEE Transactions on Smart Grid*, vol. 11, no. 3, pp. 2734-2736, May 2020.
[13] W. Zhang, X. Yan, and H. Huang, "Performance tuning for power electronic interfaces under VSG control," *Applied Sciences*, vol. 10, pp. 953, Feb. 2020.
[14] P. Tielens and D. Van Hertem, "The relevance of inertia in power systems," *Renewable & Sustainable Energy Reviews*, vol. 55, pp. 999-1009, Mar. 2016.
[15] Y. Ye, Y. Qiao, and Z. Lu, "Revolution of frequency regulation in the converter-dominated power system," *Renewable and Sustainable Energy Reviews*, vol. 111, pp. 145-156, Apr. 2019.
[16] H. J. Kim, R. Sioshansi, and A. J. Conejo, "Benefits of stochastic optimization for scheduling energy storage in wholesale electricity markets," *Journal of Modern Power Systems and Clean Energy*, vol. 9, no. 1, pp. 181-189, Jan. 2021.
[17] S. He, H. Gao, H. Tian *et al*., "A two-stage robust optimal allocation model of distributed generation considering capacity curve and real-time price based demand response," *Journal of Modern Power Systems and Clean Energy*, vol. 9, no. 1, pp. 114-127, Jan. 2021.
[18] R. A. Jabr, "Linear decision rules for control of reactive power by distributed photovoltaic generators," *IEEE Transactions on Power Systems*, vol. 33, no. 2, pp. 2165-2174, Mar. 2018.
[19] A. Papavasiliou, S. S. Oren, and B. Rountree, "Applying High performance computing to transmission-constrained stochastic unit commitment for renewable energy integration," *IEEE Transactions on Power Systems*, vol. 30, no. 3, pp. 1109-1120, May 2015.
[20] J. Wang, M. Shahidehpour, and Z. Li, "Security-constrained unit commitment with volatile wind power generation," *IEEE Transactions on Power Systems*, vol. 23, no. 3, pp. 1319-1327, Aug. 2008.
[21] D. Bertsimas, E. Litvinov, X. Sun *et al*., "Adaptive robust optimization for the security constrained unit commitment problem," *IEEE Transactions on Power Systems*, vol. 28, no. 1, pp. 52-63, Feb. 2013.
[22] R. Doherty and M. O'Malley, "A new approach to quantify reserve demand in systems with significant installed wind capacity," *IEEE Transactions on Power Systems*, vol. 20, no. 3, pp. 587-595, May 2005.
[23] H. Holttinen, M. Milligan, E Ela *et al*., "Methodologies to determine operating reserves due to increased wind power," *IEEE Transactions on Sustainable Energy*, vol. 3, no. 4, pp. 713-723, Oct. 2012.
[24] H. Huang, M. Zhou, and G. Li, "An endogenous approach to quantifying the wind power reserve," *IEEE Transactions on Power Systems*, vol. 35, no. 3, pp. 2431-2442, Nov. 2020.
[25] H. Huang, M. Zhou, L. Zhang *et al*., "Joint generation and reserve scheduling of wind-solar-pumped storage power systems under multiple uncertainties," *International Transactions on Electrical Energy Systems*, vol. 29, pp. 777-795, Apr. 2019.
[26] L. Roald, G. Andersson, S. Misra *et al*., "Optimal power flow with wind power control and limited expected risk of overloads," in *Proceedings of 2016 Power Systems Computation Conference (PSCC)*, Genoa, Italy, Jun. 2016, pp. 1-7.
[27] M. Vrakopoulou, K. Margellos, J. Lygeros *et al*., "A probabilistic framework for reserve scheduling *N*–1 and security assessment of systems with high wind power penetration," *IEEE Transactions on Power Systems*, vol. 28, no. 4, pp. 3885-3896, Jul. 2013.
[28] M. Vrakopoulou, B. Li, and J. M. Chance, "Constrained reserve scheduling using uncertain controllable loads Part I: formulation and scenario-based analysis," *IEEE Transactions on Smart Grid*, vol. 10, no. 2, pp. 1608-1617, Nov. 2019.
[29] F. Teng, V. Trovato, and G. Strbac, "Stochastic scheduling with inertia-dependent fast frequency response requirements," *IEEE Transactions on Power Systems*, vol. 31, no. 3, pp. 1557-1566, Jun. 2016.
[30] K. Hansen, C. Breyer, and H. Lund, "Status and perspectives on 100% renewable energy systems," *Energy*, vol. 175, pp. 471-480, Mar. 2019.
[31] A. M. Massoud, S. Ahmed, S. J. Finney *et al*., "Inverter-based versus synchronous-based distributed generation: fault current limitation and protection issues," in *Proceedings of 2010 IEEE Energy Conversion Congress and Exposition*, Atlanta, USA, Nov. 2010, pp. 1-6.
[32] W. Zhang, X. Yan, and H. Huang, "Adaptive performance tuning for voltage-sourced converters with frequency responses," *Applied Sciences*, vol. 10, no. 5, pp. 1884-1903, Mar. 2020.
[33] J. Rocabert, A. Luna, F. Blaabjerg *et al*., "Control of power converters in AC microgrids," *IEEE Transactions on Power Electronics*, vol. 27, no. 11, pp. 4734-4749, May 2012.
[34] Y. Ye, L. Wei, J. Ruan *et al*., "A generic reduced-order modeling hierarchy for power-electronic interfaced generators with the quasi-constant-power feature," *Proceedings of the CSEE*, vol. 37, no. 14, pp. 3993-4001, Jul. 2017.
[35] H. Wu, X. Ruan, D. Yang *et al*., "Small-signal modeling and parameters design for virtual synchronous generators," *IEEE Transactions on Industrial Electronics*, vol. 63, no. 7, pp. 4292-4303, Jul. 2016.
[36] J. Fang, H. Li, Y. Tang *et al*., "Distributed power system virtual inertia implemented by grid-connected power converters," *IEEE Transactions on Power Electronics*, vol. 33, no. 10, pp. 8488-8499, Oct. 2018.
[37] L. M. Castro, C. R. Fuerte-Esquivel, and J. H. Tovar-Hernandez, "Solution of power flow with automatic load-frequency control devices including wind farms," *IEEE Transactions on Power Systems*, vol. 27, no. 4, pp. 2186-2195, Nov. 2012.
[38] P. Kundur, J. Paserba, V. Ajjarapu *et al*., "Definition and classification of power system stability IEEE/CIGRE joint task force on stability terms and definitions," *IEEE Transactions on Power Systems*, vol. 19, no. 3, pp. 1387-1401, Aug. 2004.
[39] P. Chilukuri, S. R. Narasimhan, N. Nallarasan *et al*., "Introduction of secondary frequency control in Indian power system," in *Proceedings of the 20th National Power Systems Conference*, Tiruchirappalli, India, Dec. 2018, pp. 1-6.
[40] J. Wang, M. Shahidehpour, and Z. Li, "Contingency-constrained reserve requirements in joint energy and ancillary services auction," *IEEE Transactions on Power Systems*, vol. 24, no. 3, pp. 1457-1468, Aug. 2009.
[41] B.-M. Hodge and M. Milligan, "Wind power forecasting error distributions over multiple timescales," in *Proceedings of IEEE PES General Meeting*, Detroit, USA, Jul. 2011, pp. 1-8.

Weichao Zhang received the B.S., M.S., and Ph.D. degrees in North China Electric Power University, Beijing, China, in 2009, 2013, and 2021, respectively. He is now working in the Internship at China Electric Power Research Institute, Beijing, China. His main research interests include the operation and control of power systems with renewable integration.

Wanxing Sheng received the Ph.D. degree in electronic engineering from Xi'an Jiaotong University, Xi'an, China, in 1995. He engaged in scientific research in power system automation, distribution network, distributed power generation and micro-grid, energy Internet, etc. His main research interests include operation and planning of power distribution systems.

Qing Duan received the M.S. degree in School of Computer Science, Hua-

zhong University of Science and Technology, Wuhan, Chian, and the Ph.D. degree in School of Electrical Engineering, Shandong University, Jinan, China. He is now a Post-doctorate in China Electric Power Research Institute, Beijing, China, engaged in research work on intelligent distribution system planning, operation control, power electronics technology, artificial intelligence and equipment research and development. His main research interests include advanced power distribution systems.

Hanyan Huang received the B. S. degree in electrical engineering from North China Electric Power University, Beijing, China, in 2016. She is currently working toward the Ph.D. degree in electrical engineering with North China Electric Power University. Her main research interests include power system operation with integration of renewable sources.

Xiangwu Yan received the B. S. degree in electrical engineering from Hunan University, Changsha, China, in 1986, the M.S. degree from North China Electric Power University, Baoding, China, in 1990, and the Ph. D. degree from the Harbin Institute of Technology, Harbin, China, in 1997. He was an Honorary Fellow of the Wisconsin Electric Machines and Power Electronics Consortium (WEMPEC) with the University of Wisconsin-Madison, Madison, USA. Then, he returned to the North China Electric Power University as a Faculty Member, where he continues to direct research in various areas of electronic power conversion. His main research interests include power electronics and wind power.